

1  
2       **A link between the hiatus in global warming and North American drought**  
3

4       Thomas L. Delworth<sup>1</sup>, Fanrong Zeng<sup>1</sup>, Anthony Rosati<sup>1,2</sup>, Gabriel Vecchi<sup>1</sup>, and Andrew Wittenberg<sup>1</sup>  
5

6                   <sup>1</sup>Geophysical Fluid Dynamics Laboratory/NOAA  
7

8                   201 Forrestal Rd.  
9

10                  Princeton, NJ 08540 USA  
11

12                  <sup>2</sup>University Corporation for Atmospheric Research (UCAR)  
13

14                  Accepted, *Journal of Climate*  
15

16                  February 22, 2015  
17

18  
19  
20  
21       Corresponding author: Thomas L. Delworth  
22

23       E-Mail: tom.delworth@noaa.gov  
24       Phone: 609-452-6565  
25

26       Postal:  
27       Geophysical Fluid Dynamics Laboratory/NOAA  
28       201 Forrestal Rd.  
29       Princeton University Forrestal Campus  
30       Plainsboro, NJ 08540  
31       USA  
32

33

34  
35

## Abstract

36 Portions of western North America have experienced prolonged drought over the last decade.  
37 This drought has occurred at the same time as the global warming hiatus – a decadal period  
38 with little increase in global mean surface temperature. We use climate models and  
39 observational analyses to clarify the dual role of recent tropical Pacific changes in driving both  
40 the global warming hiatus and North American drought. When we insert observed tropical  
41 Pacific wind stress anomalies into coupled models, the simulations produce persistent  
42 negative sea surface temperature anomalies in the eastern tropical Pacific, a hiatus in global  
43 warming, and drought over North America driven by SST-induced atmospheric circulation  
44 anomalies. In our simulations the tropical wind anomalies account for 92% of the simulated  
45 North American drought during the recent decade, with 8% from anthropogenic radiative  
46 forcing changes. This suggests that anthropogenic radiative forcing is not the dominant driver  
47 of the current drought, unless the wind changes themselves are driven by anthropogenic  
48 radiative forcing. The anomalous tropical winds could also originate from coupled interactions  
49 in the tropical Pacific or from forcing outside the tropical Pacific. The model experiments  
50 suggest that if the tropical winds were to return to climatological conditions, then the recent  
51 tendency toward North American drought would diminish. Alternatively, if the tropical winds  
52 were to persist, then the impact on North American drought would continue; however, the  
53 impact of the enhanced Pacific easterlies on global temperature diminishes after a decade or  
54 two due to a surface reemergence of warmer water that was initially subducted into the ocean  
55 interior.

56

57 **1. Introduction**

58 There has been a prolonged drought over portions of western North America since around the year  
59 2000 (Stahle et al. 2009; Cayan et al. 2010; Seager and Hoerling 2014), encompassing regions from  
60 the western Plains to the West Coast. This decadal-scale drought has created substantial impacts in  
61 many societal sectors, including agriculture and wildfires (Dennison et al. 2014). The underlying  
62 causes of the drought are not well established in terms of the role of natural variability versus human-  
63 induced radiative forcing changes, such as from increasing greenhouse gases. Recent work focusing  
64 on California drought during the shorter 2011-2014 period has suggested that internal variability is  
65 likely responsible (Wang and Schubert 2014a; Funk et al. 2014; Seager et al. 2015), although aspects  
66 of the atmospheric circulation associated with that drought could have some relationship to climate  
67 change (Swain et al. 2014). The causes of the larger-scale decadal drought over western North  
68 America are less clear. This decadal-scale drought has occurred at the same time as the so-called  
69 global warming hiatus(Easterling and Wehner 2009; Bindoff, N.L., et al. 2013; Hawkins et al. 2014), a  
70 decadal period with little increase in global mean surface temperature. In this study we find a clear  
71 link between the hiatus and recent decadal-scale drought over portions of North America via  
72 enhanced easterly winds in the tropical Pacific and their association with decadal changes in local sea-  
73 surface temperature.

74

75 There are a number of factors that could have contributed to the recent observed hiatus in global  
76 warming (Clement and DiNezio 2014), including natural radiative forcing, anthropogenic radiative  
77 forcing, and internal variability of the climate system. Potential natural radiative forcing factors  
78 include volcanic activity (Santer et al. 2014) and a persistently low level of solar irradiance in the  
79 most recent solar cycle, in addition to changes in stratospheric water vapor(Solomon et al. 2010). An

80 altered vertical distribution of heating within the ocean could have also contributed to the hiatus  
81 (Trenberth and Fasullo 2013; Katsman and van Oldenborgh 2011; Balmaseda et al. 2013). The hiatus  
82 could also have substantial contributions from internal variability of the coupled system, linked to  
83 phenomena such as ENSO and the Pacific Decadal Oscillation(Meehl et al. 2011, 2013; Vecchi and  
84 Wittenberg 2010; Ogata et al. 2013) or the Atlantic Multidecadal Oscillation(Tung and Zhou 2013). It  
85 has also been suggested that incomplete coverage in observing systems(Cowtan and Way 2014) could  
86 have led to underestimation of the true warming trend.

87

88 Recent work has highlighted the importance of observed changes in the tropical Pacific for explaining  
89 the hiatus in global warming. Kosaka and Xie (2013) were able to simulate the hiatus using a global  
90 climate model when sea surface temperatures (SSTs) over the eastern near-equatorial Pacific were  
91 strongly damped towards observed SSTs. England et al. (2014) extended this work by first noting that  
92 the hiatus period has exhibited unusually intense easterly winds in the tropical Pacific. They then  
93 showed that these enhanced easterly winds in the Pacific lead a climate model to replicate many  
94 aspects of the observed hiatus, including global mean surface air temperature and the patterns of  
95 upper ocean heat content change. Taken together, Kosaka and Xie (2013) and England et al. (2014)  
96 indicate that much of the hiatus may be connected to tropical Pacific SST and wind stress changes.  
97 Recent work has suggested that the enhanced tropical Pacific easterly winds could be partly driven  
98 from regions outside the Pacific, whether from the Indian Ocean (Luo et al. 2012) or the Atlantic  
99 (McGregor et al. 2014).

100

101 In the current study we use numerical modeling experiments to explore the relationships between  
102 enhanced tropical Pacific easterly winds and global climate. The results of our experiments, done with

103 a suite of different models, independently confirm the results of England et al (2014) and support the  
104 conclusions of Kosaka and Xie (2013). Further, we show a strong connection between these same  
105 tropical Pacific wind stress changes and drought over North America. Our results suggest that the  
106 observed drought over portions of western North America over the last decade is not likely to be a  
107 direct response of the climate system to radiative forcing changes, unless the wind stress changes  
108 themselves are induced by radiative forcing changes. We also show, using idealized experiments, that  
109 the impact of constant easterly tropical Pacific wind anomalies on simulated global-mean  
110 temperature appears to be transient, diminishing after a decade or two.

111 **2. Model, simulations, and observational data**

112 **a. Model and simulations**

113 We use targeted numerical experiments with multiple comprehensive climate models in concert with  
114 observational analyses. We use three models: (a) the Geophysical Fluid Dynamics Laboratory (GFDL)  
115 CM2.1 model(Delworth et al. 2006; Wittenberg et al. 2006); (b) the GFDL CM2.5\_FLOR model (Vecchi  
116 et al. 2014), hereafter referred to as “FLOR”; and (c) the GFDL CM2.5\_FLOR\_FA model (Vecchi et al.  
117 2014), hereafter referred to as FLOR\_FA. All three models share many aspects of their physics, and  
118 have very similar ocean models, but differ in atmospheric resolution. The CM2.1 model has an  
119 atmospheric horizontal grid-spacing of ~200 Km, with 24 vertical levels. The FLOR and FLOR\_FA  
120 models derive from the GFDL CM2.5 model (Delworth et al. 2012), and have atmospheric grid-spacing  
121 of ~50 Km in the horizontal, with 32 levels in the vertical, and a more sophisticated land model than  
122 the CM2.1 model. The FLOR\_FA model differs from FLOR through the use of flux adjustments  
123 (Magnusson et al. 2013) as a numerical technique to reduce climatological model biases, while  
124 allowing the model to generate internal variability and respond to radiative forcing. The CM2.1 and

125 FLOR models are used in routine seasonal prediction as part of the North American MultiModel  
126 Ensemble (Kirtman et al. 2013).

127

128 We use several types of experiments. Experiments using CM2.1 are ten-member ensembles, while  
129 experiments using FLOR and FLOR\_FA are five-member ensembles

130 (1) CONTROL: These simulations use concentrations of greenhouse gases and other radiative forcing  
131 components that are constant at preindustrial conditions (approximately calendar year 1860).

132 (2) CONTROL\_STRESS: These simulations are conducted as departures from the Control simulation,  
133 but in which a uniform zonal wind stress anomaly (-0.008 N m<sup>-2</sup>) over a rectangular domain in the  
134 Tropical Pacific is *added* to the momentum flux into the ocean calculated by the coupled model from  
135 air-sea gradients. The domain for the stress addition extends from 15°S to 15°N, with a 10° buffer  
136 zone on the northern and southern sides where the stress anomalies taper linearly to zero at +/- 25°  
137 latitude; in longitude the domain extends from 150°E to the coast of South America, with a 10° buffer  
138 zone from 140°E to 150°E. These simulations are 100 years long.

139 (3) ALLFORC: These simulations cover the period from 1861 to 2040, using estimates of the observed  
140 changes in radiative forcing over the 1861-2005 period, and with estimated changes in radiative  
141 forcing for 2006-2040 based on the Radiative Concentration Pathways scenario 4.5 (RCP4.5; see  
142 <http://cmip-pcmdi.llnl.gov/cmip5/forcing.html> for details).

143 (4) ALLFORC\_STRESS: These simulations are identical to ALLFORC, except that the model calculated  
144 wind stress anomalies that the ocean feels are replaced over the tropical Pacific (region shown in Fig.  
145 1b) with stress anomalies derived from European Center for Medium Range Weather Forecasting  
146 (ECMWF) reanalysis (Dee et al. 2011) on a month by month basis over the period 1979-2013. This  
147 replacement occurs only over the tropical Pacific, and only affects the momentum flux. The

148 differences between ALLFORC\_STRESS and ALLFORC experiments represent the impacts on the  
149 global climate system of the momentum flux into the ocean from observed tropical Pacific wind stress  
150 anomalies over the period 1979-2013.

151

152 More specifically, we replace the model calculated wind stress at each time step with a stress value  
153 from an imposed wind stress time series. This time series is composed of three parts: (a) daily wind  
154 stress values from the ALLFORC simulation that have been filtered to retain only time scales shorter  
155 than 30 days, (b) a repeating seasonal cycle of wind stress calculated from the ALLFORC experiment,  
156 and (c) monthly wind stress perturbations derived from the ECMWF Interim Reanalysis (Dee et al.  
157 2011). These perturbations are calculated as the anomalies from their climatological seasonal cycle  
158 computed over the 1979-2013 period - this ensures that the time-mean of the reanalysis wind stress  
159 anomalies applied to the CM2.1 model is zero over the 1979-2013 period. The above construction  
160 conserves the time-mean of the wind stress time series from the original coupled model, so as not to  
161 induce a model drift, but still allows the model to feel interannual wind stress variations similar to  
162 observational estimates over this period. For the Pacific there is a complete replacement of the wind  
163 stress in the deep Tropics ( $15^{\circ}\text{S}$ - $15^{\circ}\text{N}$ ); from  $25^{\circ}\text{S}$ - $15^{\circ}\text{S}$  and  $15^{\circ}\text{N}$ - $25^{\circ}\text{N}$  the wind stress is a mixture of  
164 the model's calculated wind stress and the replacement time series, with a linear taper such that the  
165 replacement effect goes to zero at  $25^{\circ}\text{S}$  and  $25^{\circ}\text{N}$ . Poleward of  $25^{\circ}$  the model stresses are computed  
166 entirely by the model based on air-sea gradients and then passed to the ocean component. In this  
167 process we only alter the flux of momentum through the stress field – the wind effects on latent and  
168 sensible heat fluxes are unaltered, and are computed based on the model's internal physics.

169

170 We show the time series (Fig. 1a) and spatial pattern (Fig. 1b) of the tropical Pacific wind stress  
171 anomalies imposed in the ALLFORC\_STRESS experiments. The primary characteristic is an  
172 enhancement of the easterly winds from the late 1990s onward. The ALLFORC\_STRESS simulations  
173 are able to largely replicate the observed timings of El Niño and La Niña events (Fig. 2) in response to  
174 the imposed wind stress anomalies, although the simulated amplitude of SST variations is larger than  
175 observed. The simulation of ENSO in FLOR\_FA is notably more realistic than in FLOR (Vecchi et al.  
176 2014), with a more realistic amplitude and seasonal phase locking than in FLOR or CM2.1.

177

178 We note that within the tropical Pacific, the zonal wind stress is tightly coupled to the zonal SST  
179 gradient and zonal thermocline slope. Thus in the above experiments, the wind stress can be viewed  
180 as a proxy for the state of the tropical Pacific ocean and atmosphere. Prescribing the wind stress  
181 anomalies in this region is one method to prescribe the full decadal state of the tropical Pacific, which  
182 then permits an assessment of the Pacific's downstream impacts on the rest of the globe.

183

184 **b. Observational data**

185 The observed monthly precipitation data(Harris et al. 2014) comes from the Climatic Research Unit  
186 (CRU) of the University of East Anglia. The data is global on a  $0.5^{\circ}$  grid, extending from 1901 through  
187 2012. The observed monthly surface air temperature (HADCRU4) (Jones et al. 2012) also comes from  
188 CRU, and is on a  $5^{\circ}$  grid, extending from 1850 to the present. The surface wind stresses come from the  
189 European Center for Medium Range Weather Forecasting (ECMWF)-Interim Reanalysis(Dee et al.  
190 2011).

191

192 **3. Results**

193 **a. Temperature response**

194 The simulations are able to capture many aspects of the hiatus in response to these winds (Fig. 3a).  
195 The observed record shows the 2002-2013 hiatus period with little trend in global mean surface air  
196 temperature. The ALLFORC ensemble continues warming throughout the period. In contrast, the  
197 ALLFORC\_STRESS ensemble has considerably reduced warming after the year 2002, demonstrating  
198 that it has replicated aspects of the observed hiatus in response to the strengthening of the tropical  
199 Pacific easterly winds, similar to England et al. (2014). While the ALLFORC\_STRESS ensemble mean  
200 warming trend is still larger than the observations (for CM2.1 and FLOR), the decadal temperature  
201 trends in the ALLFORC\_STRESS ensemble members using the three models are systematically smaller  
202 than in the corresponding ALLFORC ensembles (Fig. 3b). In particular, the observed trend lies near  
203 the center of the distribution of trends from the ALLFORC\_STRESS runs using FLOR\_FA.

204

205 We show in Fig. 4 the patterns of surface and subsurface ocean temperature change in response to the  
206 imposed wind stress changes using the CM2.1 model for the ALLFORC\_STRESS and CONTROL\_STRESS  
207 experiments (we obtain similar results using the FLOR and FLOR\_FA models, not shown). By  
208 increasing upwelling and vertical mixing, and strengthening the zonal tilt of the equatorial  
209 thermocline, the enhanced easterly winds force cold, subsurface water in the eastern tropical Pacific  
210 to the surface. The enhanced winds also depress the thermocline in the western tropical Pacific, and  
211 force warm near-surface water in the tropical western Pacific to subduct into the ocean interior; this  
212 leads to positive subsurface temperature anomalies in the western tropical Pacific (Figs. 4b and 4d).  
213 The exposure of the cold water to the atmosphere in the eastern Pacific, combined with the  
214 movement of warmer surface water into the subsurface ocean in the western Pacific, contributes to

215 the hiatus. In contrast, the pattern of SST change that occurs solely in response to radiative forcing  
216 changes (Fig. 5) is much more uniform.

217 **b. Precipitation response**

218 How are these enhanced easterlies and the hiatus connected to North American drought? It has been  
219 known for some time that SST in the Pacific can influence precipitation over North America  
220 (Ropelewski and Halpert 1986; Trenberth et al. 1988; Hoerling 2003; Seager et al. 2005; Schubert et  
221 al. 2004, 2009; Findell and Delworth 2010; Seager and Hoerling 2014; Wang and Schubert 2014b). In  
222 particular, cold ocean temperature anomalies in the eastern tropical Pacific have been linked with  
223 anomalously dry conditions over parts of North America. We therefore examine whether these stress-  
224 induced Pacific SST changes induce precipitation anomalies over North America.

225

226 We first examine (Fig. 6) the ability of the models to simulate annual mean climatological  
227 precipitation over North America. The higher resolution models (FLOR and FLOR\_FA) simulate a  
228 more realistic spatial pattern and magnitude of annual mean precipitation than the lower resolution  
229 CM2.1 model. In addition, the model using flux adjustments (FLOR\_FA) has the most realistic  
230 simulation of annual mean precipitation among the models, including a more realistic depiction of the  
231 east-west precipitation gradients from Texas through the Great Plains. Biases in the model's  
232 simulation of ocean temperature contribute to the biases in continental precipitation over North  
233 America (and for other continents, not shown).

234

235 We show in Figure 7 changes in annual mean precipitation (2002-2012 minus 1979-2000) for the  
236 observations (Fig. 7a), and for the ALLFORC\_STRESS simulations (Fig. 7b-d). The observed tendency  
237 for reduced precipitation in western North America (Fig. 7a) is reproduced in the ALLFORC\_STRESS

238 experiments with each model (Fig. 7b-d). Averaged over the region  $130^{\circ}\text{W}$ - $95^{\circ}\text{W}$ , and  $30^{\circ}\text{N}$ - $42^{\circ}\text{N}$ , the  
239 reduction in observed precipitation is  $0.137 \text{ mm day}^{-1}$ . For models CM2.1, FLOR, and FLOR\_FA the  
240 simulated reductions over this region (land only) are 0.102, 0.095, and  $0.117 \text{ mm day}^{-1}$ , respectively.  
241 Since these experiments contain both radiative forcing changes and wind stress changes, we ask  
242 whether the tendency for reduced precipitation is due to radiative forcing changes or to the effects of  
243 tropical Pacific wind stress changes. We estimate the wind-forced component as the difference in  
244 precipitation between the ALLFORC\_STRESS and ALLFORC experiments for the 2002-2012 period.  
245 We also estimate the radiatively forced component as the precipitation in ALLFORC for the 2002-  
246 2012 period minus the 1979-2000 period. Combining the results of all three models, the wind-stress  
247 forcing accounts for 92% of the reduction in simulated annual mean precipitation, with the  
248 radiatively forced component accounting for 8%. A number of model-based studies (see, for example,  
249 (Seager et al. 2007; Cayan et al. 2010)) have shown that aridity may increase over southwestern  
250 North America in response to increasing greenhouse gases and the resultant warming of the planet,  
251 and from associated factors such as the expansion of the Hadley cell(Lu et al. 2007). However, the  
252 current results suggest that such factors were not primary drivers of the recent drought, consistent  
253 with earlier results (Hoerling et al. 2010; Seager and Naik 2012).

254

255 The tropical SST anomaly pattern creates a tendency for an atmospheric circulation pattern that is  
256 conducive to drought, but atmospheric internal dynamics also influence whether or not a drought  
257 occurs. Given this important role for atmospheric internal variability, we evaluate the likelihood of a  
258 change in precipitation in a more probabilistic framework. We first note that for the period 1979-  
259 2000 we have 220 individual years for the CM2.1 ALLFORC ensemble (22 years times ten ensemble  
260 members), and 220 total years for the ALLFORC ensembles using both FLOR and FLOR\_FA (22 years

times five ensemble members times two models). For each model time series we compute an areal mean over the region  $130^{\circ}\text{W}$ - $95^{\circ}\text{W}$  and  $30^{\circ}\text{N}$ - $42^{\circ}\text{N}$  (land only). We consider all of the model output for the period 1979-2000 to be one “population” (440 points). We then randomly sample this population, drawing eleven samples at a time and then computing an eleven-year mean (the same length as the 2002-2012 period). We repeat this process 10,000 times to form a distribution of decadal mean precipitation anomalies consistent with the 1979-2000 period for these models, and show that in Figure 8 as a cumulative distribution function. We do the same with output from the ALLFORC\_STRESS ensembles over this same period. These two distributions are very similar, indicating similar likelihoods of dry and wet decades from the ALLFORC and ALLFORC\_STRESS ensembles for the 1979-2000 period. We then repeat this process using output for the period 2002-2012 from the ALLFORC ensemble. We see (Fig. 8) that the distribution for 2002-2012 from the ALLFORC ensemble has been displaced slightly to the left, indicating a small increased likelihood of negative decadal-mean precipitation anomalies in response to radiative forcing changes. We next repeat this process for the ALLFORC\_STRESS output from 2002-2012. We find a much larger movement of the distribution to the left, indicating a substantial increase in the likelihood of dry decades in response to enhanced tropical easterly winds. It is still quite possible to have a decade with above average precipitation in the ALLFORC\_STRESS simulations, but the likelihood of such a decade has dropped substantially. These model results therefore suggest that the sustained easterly wind anomalies over the tropical Pacific, through their relationship with local sea surface temperature, created conditions that greatly increased the likelihood of drought over parts of western North America over the last decade, with an additional smaller role for radiative forcing changes in these models.

283

284 We find through examination of multi-millennial control simulations that the magnitude and duration  
285 of the easterly wind stress anomaly seen over the last decade in the tropical Pacific is unprecedented  
286 based on this model's control run internal variability, consistent with England et al (2014). This  
287 suggests several possibilities – (i) the models do not simulate sufficient decadal-scale internal  
288 variability, (ii) the observed event over the last decade is so rare that longer model simulations would  
289 be needed to realize such an event, or (iii) or the easterly wind stress anomaly has some contribution  
290 from radiative forcing that is not dominant in these models (Clement et al. 1996; Compo and  
291 Sardeshmukh 2009; Solomon and Newman 2012).

292

#### 293 **4. Discussion and potential future changes**

294 The strong connection between the intensification of Pacific trades and the drying in western North  
295 America observed over the past decade suggests that this drying cannot be connected in a  
296 straightforward fashion to greenhouse gas increases. In most coupled GCM simulations  
297 anthropogenic forcing produces a long-term *weakening* of the Walker circulation and tropical Pacific  
298 trade winds, but with substantial intrinsically-generated variability on decadal scales (Vecchi et al.  
299 2006). Therefore, unless it can be shown that the strengthened trade winds are a result of either  
300 natural or human-induced radiative forcing changes, the model results suggest that the observed  
301 drying over the western U.S. over the last decade may be primarily due to natural variability, and  
302 therefore not necessarily a harbinger of a secular drying trend (Hoerling et al. 2010; Seager and Naik  
303 2012). These results highlight how vulnerable western North America is to severe decadal swings in  
304 hydroclimate arising from internal variations of the climate system. Recent results suggest that  
305 temperature variations in either the Indian Ocean (Luo et al. 2012) or the Atlantic Ocean (McGregor et

306 al. 2014) could act as external drivers of, or feedbacks for, the Pacific trade wind changes. It is also  
307 possible that the wind changes are due solely to coupled processes in the tropical Pacific.

308

309 To illustrate possible changes in drought over the next decade we conduct two additional  
310 experiments for the period 2014-2022 using CM2.1, both starting from the end of the  
311 ALLFORC\_STRESS experiment. In the first experiment we do not impose wind stress anomalies, and  
312 the model computes its own wind stresses for the 2014-2022 period. In the second experiment the  
313 model experiences the same sequence of wind stress anomalies that was experienced over 2005-2013  
314 (ie, with unusually strong easterly winds). In the first experiment (Fig. 9a) precipitation is much  
315 closer to its climatological normal, with interannual deviations around the long-term mean. In the  
316 second experiment (Fig. 9b) there is a tendency for continued negative precipitation anomalies over  
317 the western U.S. in response to the continued easterly wind stress anomalies in the tropical Pacific.  
318 Therefore, a significant factor over the coming decade for western U.S. water resources, and for the  
319 water managers dealing with variations in water supply, is the behavior of the winds in the tropical  
320 Pacific. Although prediction of such decadal-scale variations is challenging (Wittenberg et al. 2014), it  
321 is important to improve our understanding of the factors responsible for the wind stress anomalies  
322 observed over 2002-2013(McGregor et al. 2014). This may allow us to better characterize potential  
323 future trajectories for western U.S. water resources.

324

325 We further assess future prospects for the hiatus and North American drought using the idealized  
326 experiment CONTROL\_STRESS. In this experiment we maintain the idealized zonal wind stress forcing  
327 anomaly for 100 years, and assess the evolution of the climate system. We see (Fig. 10a) that the  
328 global cooling in response to the enhanced tropical easterlies is a transient feature, persisting in these

329 models for only a decade or two. In these simulations the initial cooling is associated with upwelling  
330 of cold subsurface water and subduction of warmer surface water into the interior. We find that after  
331 a decade or two some of this warmer water that was sequestered in the ocean interior makes its way  
332 back to the surface (Fig. 11), offsetting the cooling associated with upwelling in the eastern tropical  
333 Pacific, and therefore eliminating the global cooling signal. There is in fact a small tendency for  
334 positive global temperature anomalies, likely associated with enhanced oceanic heat uptake during  
335 the first decade or two of these simulations. In contrast, eastern tropical Pacific SST anomalies remain  
336 negative, although with somewhat reduced amplitude. These results suggest that if the hiatus in  
337 global warming is generated solely by enhanced tropical wind stress, then the duration of the hiatus is  
338 limited to of order a decade or two (at least according to this model). This time scale is determined by  
339 the processes by which positive heat anomalies that were sequestered in the upper tropical ocean can  
340 reemerge at the surface. However, despite the elimination of the global cooling, negative temperature  
341 anomalies persist in the eastern tropical Pacific (Fig. 10b), and therefore continue to create conditions  
342 conducive to drought over western North America (Fig. 10c), although with diminishing amplitude.  
343 This suggests that the drought would persist in response to a continued surface cooling in the eastern  
344 tropical Pacific, despite the cessation of the hiatus in global warming.

345

346  
347 Acknowledgements

348 We thank Drs. H. Murakami and X. Yang, along with three anonymous reviewers, for very helpful  
349 comments on earlier versions of this manuscript. HADCRU4 temperature data, were provided by the  
350 NOAA/OAR/ESRL PSD, Boulder, Colorado, USA, from their Web site at <http://www.esrl.noaa.gov/psd/>.  
351 ECMWF-Interim reanalysis data was downloaded from  
352 [http://apps.ecmwf.int/datasets/data/interim\\_full\\_moda/](http://apps.ecmwf.int/datasets/data/interim_full_moda/).

353 References

354

355 Balmaseda, M. A., K. E. Trenberth, and E. Källén, 2013: Distinctive climate signals in reanalysis of  
356 global ocean heat content: SIGNALS IN OCEAN HEAT CONTENT. *Geophys. Res. Lett.*, **40**, 1754–  
357 1759, doi:10.1002/grl.50382.

358 Bindoff, N.L., et al., 2013: *Detection and Attribution of Climate Change: from Global to Regional*.  
359 Cambridge University Press, Cambridge, United Kingdom and New York, NY, USA.,

360 Cayan, D. R., T. Das, D. W. Pierce, T. P. Barnett, M. Tyree, and A. Gershunov, 2010: Future dryness in  
361 the southwest US and the hydrology of the early 21st century drought. *Proc. Natl. Acad. Sci.*,  
362 **107**, 21271–21276.

363 Clement, A., and P. DiNezio, 2014: The Tropical Pacific Ocean--Back in the Driver's Seat? *Science*, **343**,  
364 976–978, doi:10.1126/science.1248115.

365 ——, R. Seager, M.A. Cane, and S.E. Zebiak, 1996: An ocean dynamical thermostat. *J. Clim.*, **9**, 2190–  
366 2196.

367 Compo, G. P., and P. D. Sardeshmukh, 2009: Removing ENSO-Related Variations from the Climate  
368 Record. *J. Clim.*, **23**, 1957–1978, doi:10.1175/2009JCLI2735.1.

369 Cowtan, K., and R. G. Way, 2014: Coverage bias in the HadCRUT4 temperature series and its impact on  
370 recent temperature trends: Coverage Bias in the HadCRUT4 Temperature Series. *Q. J. R.  
371 Meteorol. Soc.*, n/a – n/a, doi:10.1002/qj.2297.

- 372   Dee, D. P., and Coauthors, 2011: The ERA-Interim reanalysis: configuration and performance of the  
373       data assimilation system. *Q. J. R. Meteorol. Soc.*, **137**, 553–597, doi:10.1002/qj.828.
- 374   Delworth, T. L., and Coauthors, 2006: GFDL's CM2 global coupled climate models. Part I: Formulation  
375       and simulation characteristics. *J. Clim.*, **19**.
- 376   —, and Coauthors, 2012: Simulated Climate and Climate Change in the GFDL CM2.5 High-Resolution  
377       Coupled Climate Model. *J. Clim.*, **25**, 2755–2781, doi:10.1175/JCLI-D-11-00316.1.
- 378   Dennison, P. E., S. C. Brewer, J. D. Arnold, and M. A. Moritz, 2014: Large wildfire trends in the western  
379       United States, 1984–2011: Dennison et al.; Large wildfire trends in the western US. *Geophys.*  
380       *Res. Lett.*, **41**, 2928–2933, doi:10.1002/2014GL059576.
- 381   Easterling, D. R., and M. F. Wehner, 2009: Is the climate warming or cooling? *Geophys. Res. Lett.*, **36**,  
382       doi:10.1029/2009GL037810. <http://doi.wiley.com/10.1029/2009GL037810> (Accessed  
383       November 12, 2014).
- 384   England, M. H., and Coauthors, 2014: Recent intensification of wind-driven circulation in the Pacific  
385       and the ongoing warming hiatus. *Nat. Clim. Change*, **4**, 222–227, doi:10.1038/nclimate2106.
- 386   Findell, K. L., and T. L. Delworth, 2010: Impact of Common Sea Surface Temperature Anomalies on  
387       Global Drought and Pluvial Frequency. *J. Clim.*, **23**, 485–503, doi:10.1175/2009JCLI3153.1.
- 388   Funk, C., A. Heoll, and D. Stone, 2014: Examining the contribution of the observed global warming  
389       trend to the California droughts of 2012/2013 and 2013/2014. *Bull Amer Meteor Soc*, **95**, S11–  
390       S15.

- 391 Harris, I., P. D. Jones, T. J. Osborn, and D. H. Lister, 2014: Updated high-resolution grids of monthly  
392 climatic observations - the CRU TS3.10 Dataset: UPDATED HIGH-RESOLUTION GRIDS OF  
393 MONTHLY CLIMATIC OBSERVATIONS. *Int. J. Climatol.*, **34**, 623–642, doi:10.1002/joc.3711.
- 394 Hawkins, E., T. Edwards, and D. McNeall, 2014: Pause for thought. *Nat. Clim. Change*, **4**, 154–156.
- 395 Hoerling, M., 2003: The Perfect Ocean for Drought. *Science*, **299**, 691–694,  
396 doi:10.1126/science.1079053.
- 397 Hoerling, M., J. Eischeid, and J. Perlitz, 2010: Regional Precipitation Trends: Distinguishing Natural  
398 Variability from Anthropogenic Forcing. *J. Clim.*, **23**, 2131–2145, doi:10.1175/2009JCLI3420.1.
- 399 Jones, P. D., D. H. Lister, T. J. Osborn, C. Harpham, M. Salmon, and C. P. Morice, 2012: Hemispheric and  
400 large-scale land-surface air temperature variations: An extensive revision and an update to  
401 2010. *J. Geophys. Res.*, **117**, doi:10.1029/2011JD017139.  
402 <http://doi.wiley.com/10.1029/2011JD017139> (Accessed April 29, 2014).
- 403 Katsman, C. A., and G. J. van Oldenborgh, 2011: Tracing the upper ocean's "missing heat": TRACING  
404 THE UPPER OCEAN'S "MISSING HEAT." *Geophys. Res. Lett.*, **38**, n/a – n/a,  
405 doi:10.1029/2011GL048417.
- 406 Kirtman, B. P., and Coauthors, 2013: The North American Multi-Model Ensemble (NMME): Phase-1  
407 seasonal to interannual prediction, phase-2 toward developing intra-seasonal prediction. *Bull.*  
408 *Am. Meteorol. Soc.*, <http://journals.ametsoc.org/doi/abs/10.1175/BAMS-D-12-00050.1>  
409 (Accessed November 7, 2014).

- 410 Kosaka, Y., and S.-P. Xie, 2013: Recent global-warming hiatus tied to equatorial Pacific surface cooling.  
411           *Nature*, **501**, 403–407, doi:10.1038/nature12534.
- 412 Lu, J., G. A. Vecchi, and T. Reichler, 2007: Expansion of the Hadley cell under global warming. *Geophys.*  
413           *Res. Lett.*, **34**, doi:10.1029/2006GL028443. <http://doi.wiley.com/10.1029/2006GL028443>  
414           (Accessed November 12, 2014).
- 415 Luo, J.-J., W. Sasaki, and Y. Masumoto, 2012: Indian Ocean warming modulates Pacific climate change.  
416           *Proc. Natl. Acad. Sci.*, **109**, 18701–18706, doi:10.1073/pnas.1210239109.
- 417 Magnusson, L., M. Alonso-Balmaseda, and F. Molteni, 2013: On the dependence of ENSO simulation on  
418           the coupled model mean state. *Clim. Dyn.*, **41**, 1509–1525, doi:10.1007/s00382-012-1574-y.
- 419 McGregor, S., A. Timmermann, M. F. Stuecker, M. H. England, M. Merrifield, F.-F. Jin, and Y. Chikamoto,  
420           2014: Recent Walker circulation strengthening and Pacific cooling amplified by Atlantic  
421           warming. *Nat. Clim. Change*, doi:10.1038/nclimate2330.  
422           <http://www.nature.com/doifinder/10.1038/nclimate2330> (Accessed August 4, 2014).
- 423 Meehl, G. A., J. M. Arblaster, J. T. Fasullo, A. Hu, and K. E. Trenberth, 2011: Model-based evidence of  
424           deep-ocean heat uptake during surface-temperature hiatus periods. *Nat. Clim. Change*, **1**, 360–  
425           364, doi:10.1038/nclimate1229.
- 426 ——, A. Hu, J. M. Arblaster, J. Fasullo, and K. E. Trenberth, 2013: Externally Forced and Internally  
427           Generated Decadal Climate Variability Associated with the Interdecadal Pacific Oscillation. *J.*  
428           *Clim.*, **26**, 7298–7310, doi:10.1175/JCLI-D-12-00548.1.

- 429 Ogata, T., S.-P. Xie, A. Wittenberg, and D.-Z. Sun, 2013: Interdecadal Amplitude Modulation of El Niño–  
430 Southern Oscillation and Its Impact on Tropical Pacific Decadal Variability\*. *J. Clim.*, **26**, 7280–  
431 7297, doi:10.1175/JCLI-D-12-00415.1.
- 432 Ropelewski, C., and M. Halpert, 1986: North American Precipitation and Temperature Patterns  
433 Associated with the El Niño/Southern Oscillation (ENSO). *Mon. Weather Rev.*, **114**, 2352–2362.
- 434 Santer, B. D., and Coauthors, 2014: Volcanic contribution to decadal changes in tropospheric  
435 temperature. *Nat. Geosci.*, **7**, 185–189, doi:10.1038/ngeo2098.
- 436 Schubert, S., and Coauthors, 2009: A US CLIVAR project to assess and compare the responses of global  
437 climate models to drought-related SST forcing patterns: Overview and results. *J. Clim.*, **22**.
- 438 Schubert, S. D., M. J. Suarez, P. J. Pegion, R. D. Koster, and J. T. Bacmeister, 2004: Causes of long-term  
439 drought in the US Great Plains. *J. Clim.*, **17**.
- 440 Seager, R., and N. Naik, 2012: A Mechanisms-Based Approach to Detecting Recent Anthropogenic  
441 Hydroclimate Change\*. *J. Clim.*, **25**, 236–261, doi:10.1175/JCLI-D-11-00056.1.
- 442 ——, and M. Hoerling, 2014: Atmosphere and Ocean Origins of North American Droughts. *J. Clim.*,  
443 140404144919009, doi:10.1175/JCLI-D-13-00329.1.
- 444 ——, Y. Kushnir, C. Herweijer, N. Naik, and J. Velez, 2005: Modeling of tropical forcing of persistent  
445 droughts and pluvials over western North America: 1856–2000. *J. Clim.*, **18**.
- 446 Seager, R., and Coauthors, 2007: Model Projections of an Imminent Transition to a More Arid Climate  
447 in Southwestern North America. *Science*, **316**, 1181–1184, doi:10.1126/science.1139601.

- 448 Seager, R., M. Hoerling, H. Wang, B. Lyon, A. Kumar, J. Nakamura, and N. Henderson, 2015: Causes and  
449 predictability of the 2011-2014 California drought. *J. Clim.*, doi:Submitted.
- 450 Solomon, A., and M. Newman, 2012: Reconciling disparate twentieth-century Indo-Pacific ocean  
451 temperature trends in the instrumental record. *Nat. Clim Change*, **2**, 691–699,  
452 doi:10.1038/nclimate1591.
- 453 Solomon, S., K. H. Rosenlof, R. W. Portmann, J. S. Daniel, S. M. Davis, T. J. Sanford, and G.-K. Plattner,  
454 2010: Contributions of Stratospheric Water Vapor to Decadal Changes in the Rate of Global  
455 Warming. *Science*, **327**, 1219–1223, doi:10.1126/science.1182488.
- 456 Stahle, D. W., E. R. Cook, J. V. Diaz, F. K. Fye, D. J. Burnette, R. A. Soto, R. Seager, and R. R. Heim, 2009:  
457 Early 21st-century drought in Mexico. *Eos Trans. Am. Geophys. Union*, **90**, 89–90.
- 458 Swain, D., M. Tsiang, M. Haugen, D. Singh, A. Charland, B. Rajaratnam, and N. Diffenbaugh, 2014: The  
459 extraordinary California drought of 2013/14; character, context, and the role of climate  
460 change. *Bull Amer Meteor Soc*, **95**, S3–S7.
- 461 Trenberth, K. E., and J. T. Fasullo, 2013: An apparent hiatus in global warming? *Earth's Future*, **1**, 19–  
462 32, doi:10.1002/2013EF000165.
- 463 ——, G. W. Branstator, and P. A. Arkin, 1988: Origins of the 1988 North American Drought. *Science*,  
464 **242**, 1640–1645, doi:10.1126/science.242.4886.1640.
- 465 Tung, K.-K., and J. Zhou, 2013: Using data to attribute episodes of warming and cooling in  
466 instrumental records. *Proc. Natl. Acad. Sci.*, **110**, 2058–2063, doi:10.1073/pnas.1212471110.

- 467 Vecchi, G. A., and A. T. Wittenberg, 2010: El Niño and our future climate: where do we stand? *Wiley*  
468           *Interdiscip. Rev. Clim. Change*, n/a – n/a, doi:10.1002/wcc.33.
- 469 ——, B. J. Soden, A. T. Wittenberg, I. M. Held, A. Leetmaa, and M. J. Harrison, 2006: Weakening of  
470           tropical Pacific atmospheric circulation due to anthropogenic forcing. *Nature*, **441**, 73–76,  
471           doi:10.1038/nature04744.
- 472 Vecchi, G. A., and Coauthors, 2014: On the Seasonal Forecasting of Regional Tropical Cyclone Activity.  
473           *J. Clim.*, **27**, 7994–8016, doi:10.1175/JCLI-D-14-00158.1.
- 474 Wang, H., and S. Schubert, 2014a: Causes of the extreme dry conditions over California during early  
475           2013. *Bull Amer Meteor Soc*, **95**, S7–S11.
- 476 ——, and ——, 2014b: The Precipitation Response over the Continental United States to Cold Tropical  
477           Pacific Sea Surface Temperatures. *J. Clim.*, 140408145639001, doi:10.1175/JCLI-D-13-00453.1.
- 478 Wittenberg, A. T., A. Rosati, N.-C. Lau, and J. J. Poshay, 2006: GFDL's CM2 global coupled climate  
479           models. Part III: Tropical Pacific climate and ENSO. *J. Clim.*, **19**.
- 480 ——, ——, T. L. Delworth, G. A. Vecchi, and F. Zeng, 2014: ENSO Modulation: Is It Decadally  
481           Predictable? *J. Clim.*, **27**, 2667–2681, doi:10.1175/JCLI-D-13-00577.1.

482 Figures

483

484 Figure 1 (a) Time series of annual mean zonal wind stress applied to the model ocean in the  
485 “ALLFORC\_STRESS” experiment averaged over  $140^{\circ}\text{E}$ - $160^{\circ}\text{W}$ ,  $15^{\circ}\text{S}$ - $15^{\circ}\text{N}$ . Units are  $\text{N m}^{-2}$ . As  
486 discussed in the main text the stress values are from the ERA-Interim Reanalysis. (b) Spatial pattern  
487 of stress anomalies applied to model in “ALLFORC\_STRESS” experiment for the period 2002-2012  
488 relative to the period 1979-2000.

489

490 Figure 2 Time-longitude plots of monthly SST anomalies for observations (upper right, from the  
491 HADISST data set, Rayner et al., 2003) and models (CM2.1, FLOR, and FLOR\_FA). SST values are  
492 averaged between  $5^{\circ}\text{S}$  and  $5^{\circ}\text{N}$ . Units are K. For visual perspective, dashed green lines are drawn  
493 every 10 years.

494

495 Figure 3 (a) Time series of anomalies in global mean, annual mean surface air temperature relative to  
496 the time-mean over the period 1951-1980. Units are K. Black line denotes observations from the  
497 Climatic Research Unit (CRU) at the University of East Anglia. Red (blue) line corresponds to the  
498 ensemble mean of the CM2.1 ALLFORC (ALLFORC\_STRESS) experiments. A three-year running mean  
499 was applied to all time series. (b) Trends in global mean surface air temperature over the period  
500 2000-2012, expressed as  $\text{K decade}^{-1}$ . Red (blue) symbols for ALLFORC (ALLFORC\_STRESS)  
501 experiments. Large symbols are ensemble mean, small symbols are individual ensemble members.  
502 Experiments using models CM2.1, FLOR, and FLOR\_FA are indicated by diamonds, circles, and squares  
503 respectively.

504

505   Figure 4 (a) Spatial pattern of the SST response to imposed wind stress forcing, calculated as the time-  
506   mean over 2002-2012 in ALLFORC\_STRESS minus ALLFORC. (b) Same as (a) for temperature at  
507   200m. Units are K for both panels. (c) Same as (a), but for experiment CONTROL\_STRESS minus  
508   CONTROL. (d) Same as (b), but for experiment CONTROL\_STRESS minus CONTROL.

509

510   Figure 5 Estimate of SST response(units are K) to radiative forcing change using the ALLFORC  
511   experiment with the CM2.1 model. The estimate is calculated as the 10-member ensemble mean SST  
512   for the 2002-2012 period minus the 10-member ensemble mean SST for the 1979-2000 period. The  
513   negative values in the subpolar North Atlantic are associated with a weakening of the Atlantic  
514   Meridional Overturning Circulation.

515

516

517   Figure 6 Precipitation climatology from observations and the models. Annual-mean precipitation is  
518   shown, units are mm day<sup>-1</sup>. (a) Observations from Climatic Research Unit, University of East Anglia.  
519   (b) CM2.1 model. (c) FLOR\_FA model, (d) FLOR model.

520

521   Figure 7 (a) Difference in observed annual mean precipitation for the period 2002-2012 minus 1979-  
522   2000. Observations from the Climatic Research Unit of the University of East Anglia. Units are mm  
523   day<sup>-1</sup>. (b) Same as (a) using model results from CM2.1 ALLFORC\_STRESS, showing the combined  
524   effects of wind stress and radiative forcing changes. (c) Same as (b) using FLOR\_FA. (d) Same as (b)  
525   using FLOR.

526

527 Figure 8 Cumulative probability distribution of 11-year mean precipitation anomalies ( $\text{mm day}^{-1}$ )  
528 averaged over  $130^{\circ}\text{W}-95^{\circ}\text{W}$ ,  $30^{\circ}\text{N}-42^{\circ}\text{N}$ , land only. Grey curve (black crosses) indicates results using  
529 model values from the period 1979-2000 from experiment ALLFORC (ALLFORC\_STRESS) using all  
530 three models (CM2.1, FLOR, FLOR\_FA). Red (blue) curve denotes values from ALLFORC  
531 (ALLFORC\_STRESS) over the period 2002-2012. The distributions are generated by resampling all  
532 ensemble members from each model (CM2.1, FLOR, FLOR\_FA) for the experiment and period  
533 indicated. For example, for the grey curve we use output from all ten ensemble members of  
534 experiment ALLFORC, as well as five ensemble members each from FLOR and FLOR\_FA, over the  
535 period 1979-2000 (440 total points, based on 22 years and 10 ensemble members from CM2.1, and 5  
536 ensemble members for 22 years for FLOR and FLOR\_FA respectively). We randomly pick 11 different  
537 values from among this pool of 440 values, and then average those to form an 11-year mean, and then  
538 subtract from that the ensemble mean value over the period 1979-2000. We repeat this process  
539 10,000 times to form a distribution of 11-year mean anomalies, and plot that as a cumulative  
540 probability distribution function. We repeat this process using years 1979-2000 from  
541 ALLFORC\_STRESS, years 2002-2012 from ALLFORC, and years 2002-2012 from ALLFORC\_STRESS.  
542

543 Figure 9 Time series of simulated percentage change in annual mean precipitation relative to the  
544 1979-2000 time-mean, spatially averaged over  $130^{\circ}\text{W}-90^{\circ}\text{W}$ ,  $30^{\circ}\text{N}-42^{\circ}\text{N}$  (land only). The simulations  
545 used the CM2.1 model, were 10-member ensembles, and started from identical initial conditions at  
546 the end of experiment ALLFORC\_STRESS. (a) Precipitation change with no wind forcing anomaly in  
547 tropical Pacific. (b) Precipitation change when observed wind stress anomalies over the period 2005-  
548 2013 are applied to the model over the period 2014-2022.

549

550

551 Figure 10 Response of temperature and precipitation to sustained addition of anomalous easterly  
552 wind stress in the tropical Pacific for experiment CONTROL\_STRESS. (a) Time series of global mean  
553 surface air temperature response, calculated as global mean temperature in CONTROL\_STRESS minus  
554 CONTROL. (b) Same as (a), but for SST averaged over a portion of the tropical eastern Pacific ( $170^{\circ}\text{W}$ -  
555  $100^{\circ}\text{W}$ ,  $10^{\circ}\text{S}$ - $10^{\circ}\text{N}$ ). (c) Same as (a), but for annual mean rainfall averaged over  $130^{\circ}\text{W}$ - $90^{\circ}\text{W}$ ,  $30^{\circ}\text{N}$ -  
556  $42^{\circ}\text{N}$ , land areas only, expressed as percentage change from long-term mean.

557

558 Figure 11 Response of global mean ocean temperature to sustained addition of anomalous easterly  
559 wind stress in the tropical Pacific, calculated as experiment CONTROL\_STRESS - CONTROL. Positive  
560 values indicate a warming of the ocean in response to the anomalous easterlies.

561

562

563

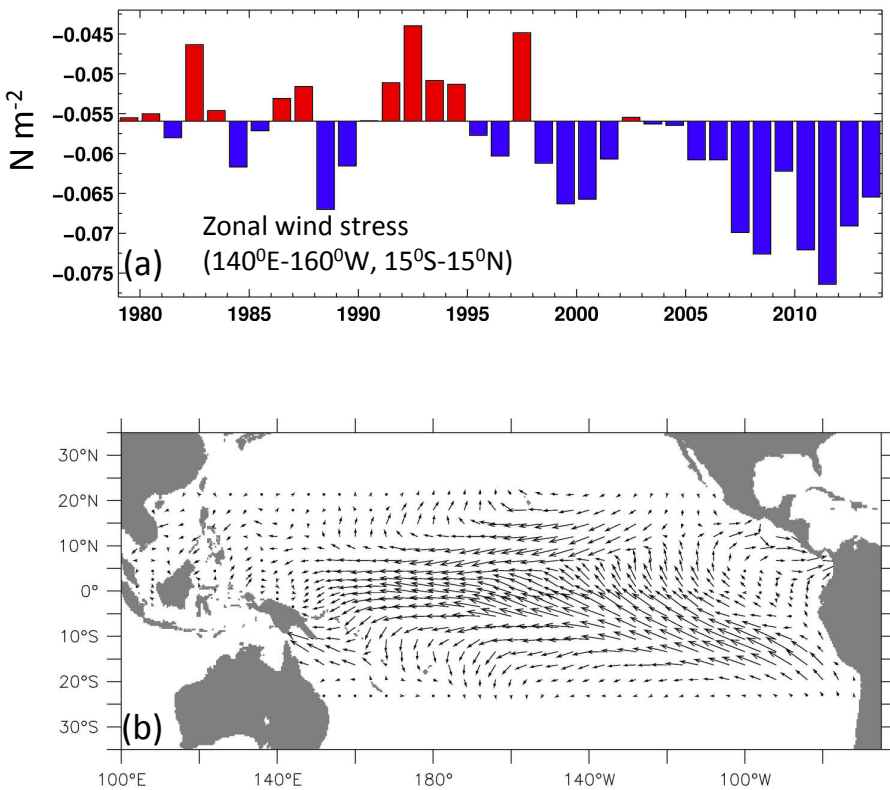


Figure 1 (a) Time series of annual mean zonal wind stress applied to the model ocean in the “ALLFORC\_STRESS” experiment averaged over  $140^{\circ}\text{E}-160^{\circ}\text{W}$ ,  $15^{\circ}\text{S}-15^{\circ}\text{N}$ . Units are  $\text{N m}^{-2}$ . As discussed in the main text the stress values are derived by combining the model’s climatological seasonal cycle with the interannual anomalies from the ERA-Interim Reanalysis. (b) Spatial pattern of stress anomalies applied to model in “ALLFORC\_STRESS” experiment for the period 2002-2012 relative to the period 1979-2000.

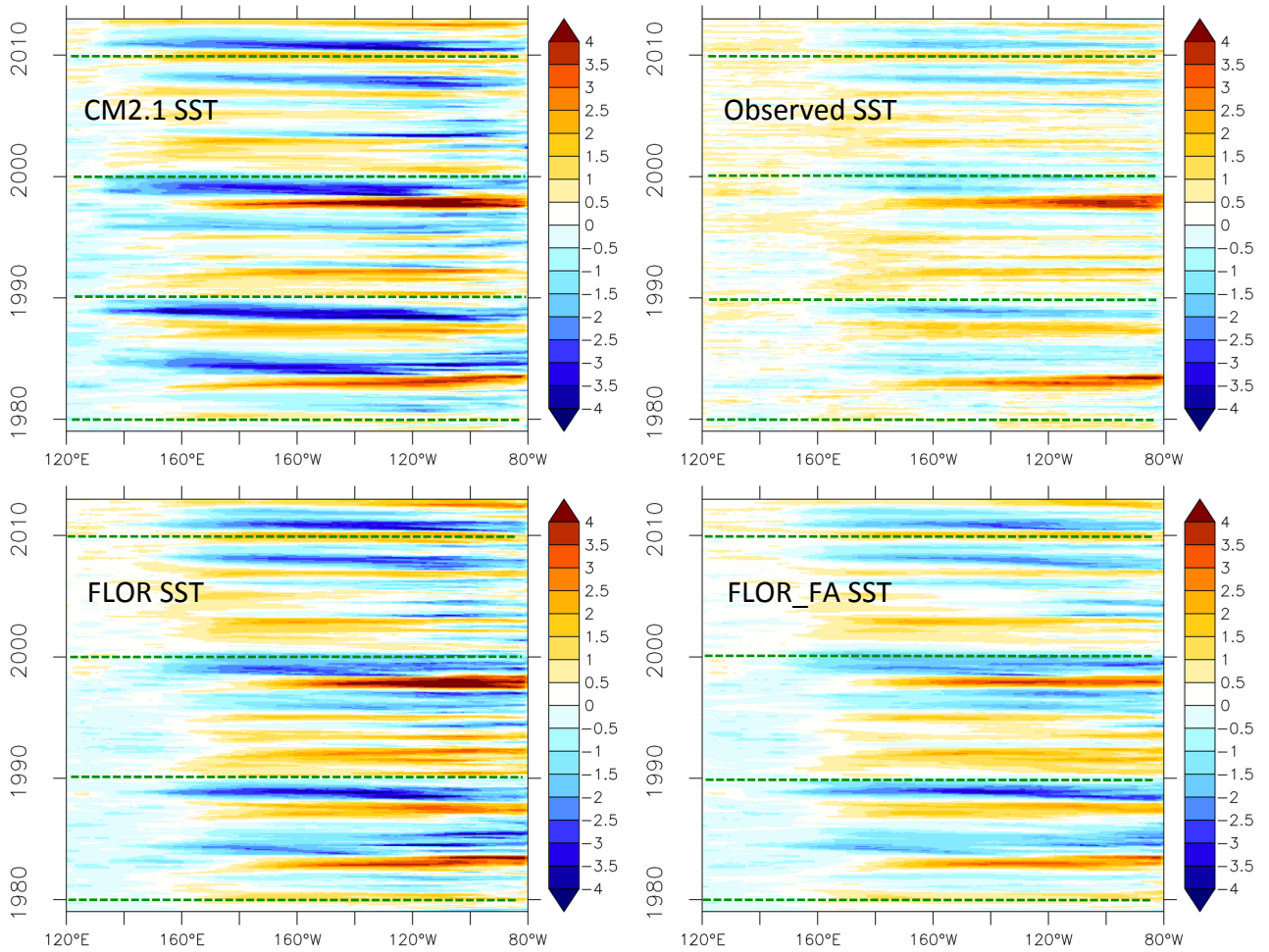


Figure 2 Time-longitude plots of monthly SST anomalies for observations (upper right, from the HADISST data set, Rayner et al., 2003) and models (CM2.1, FLOR, and FLOR\_FA). SST values are averaged between 5°S and 5°N. Units are K. For visual perspective, dashed green lines are drawn every 10 years.

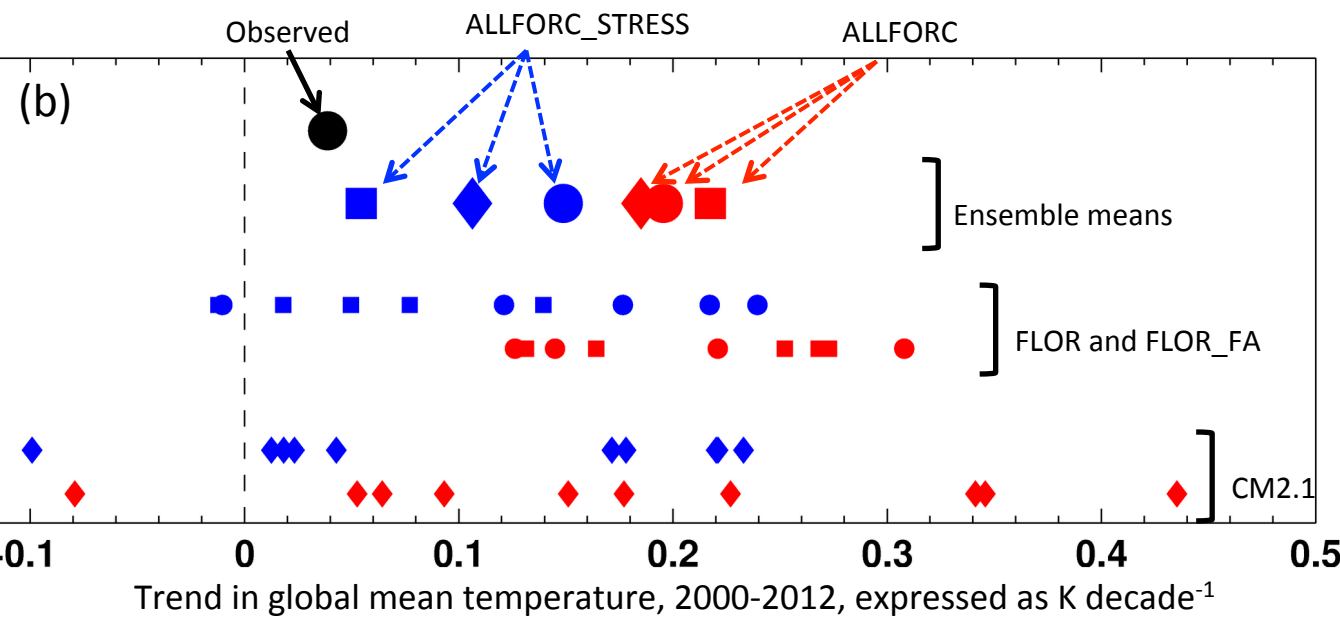
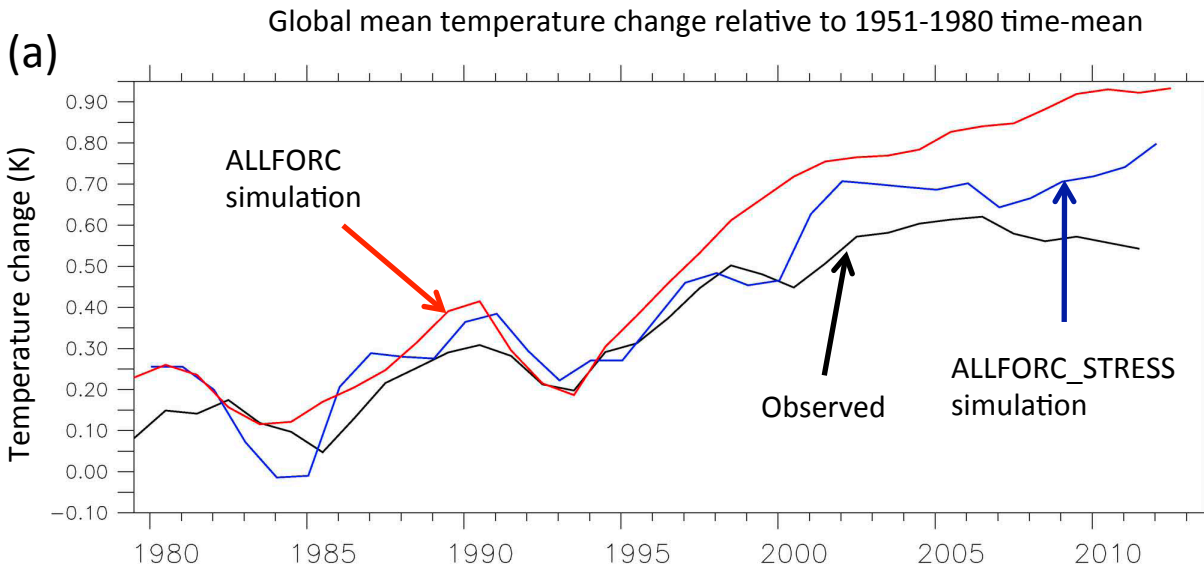


Figure 3 (a) Time series of anomalies in global mean, annual mean surface air temperature relative to the time-mean over the period 1951-1980. Units are K. Black line denotes observations from the Climatic Research Unit (CRU) at the University of East Anglia. Red (blue) line corresponds to the ensemble mean of the CM2.1 ALLFORC (ALLFORC\_STRESS) experiments. A three-year running mean was applied to all time series. (b) Trends in global mean surface air temperature over the period 2000-2012, expressed as K decade<sup>-1</sup>. Red (blue) symbols for ALLFORC (ALLFORC\_STRESS) experiments. Large symbols are ensemble mean, small symbols are individual ensemble members. Experiments using models CM2.1, FLOR, and FLOR\_FA are indicated by diamonds, circles, and squares respectively.

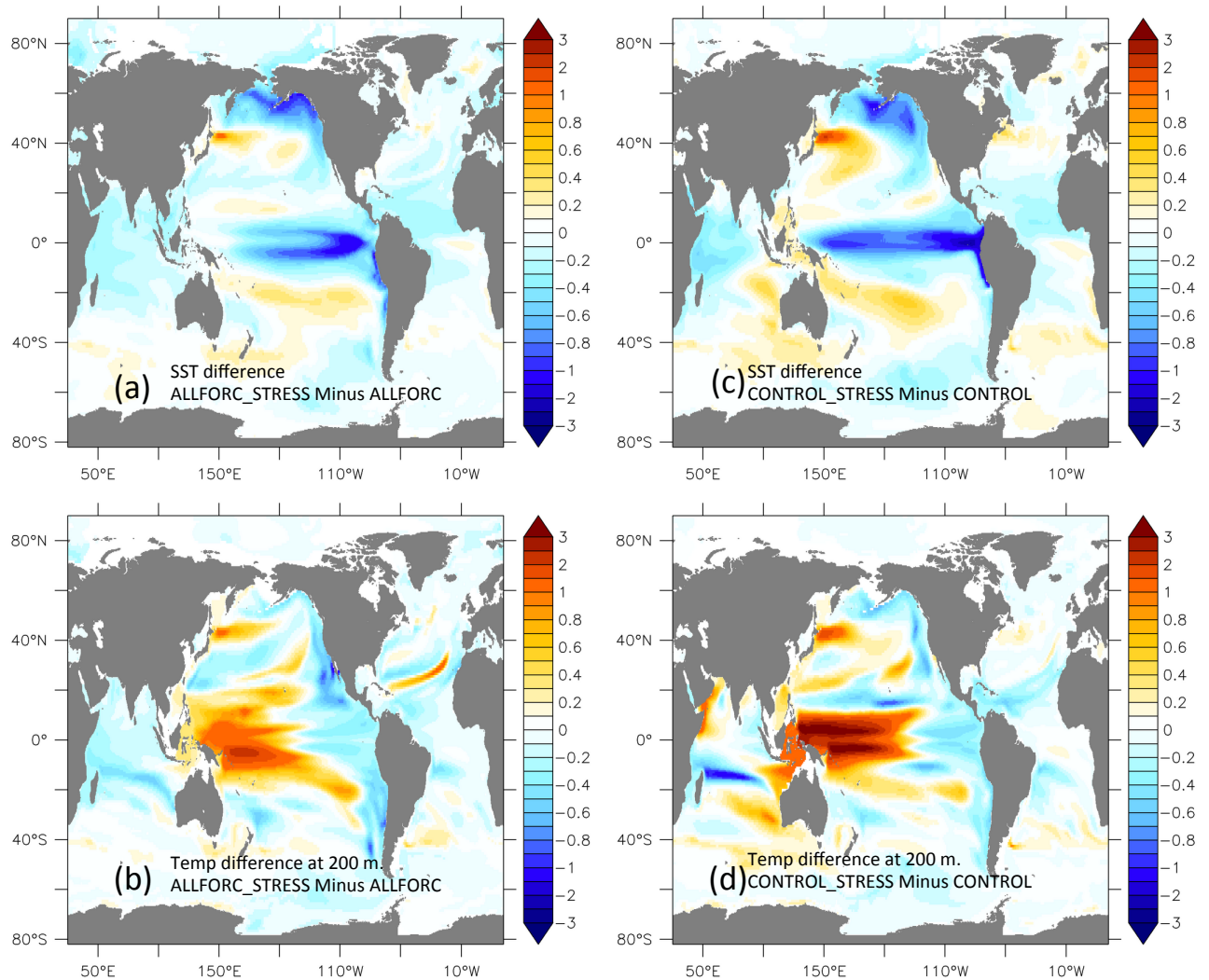


Figure 4 (a) Spatial pattern of the SST response to imposed wind stress forcing, calculated as the time-mean over 2002-2012 in ALLFORC\_STRESS minus ALLFORC. (b) Same as (a) for temperature at 200m. Units are K for both panels. (c) Same as (a), but for experiment CONTROL\_STRESS minus CONTROL. (d) Same as (b), but for experiment CONTROL\_STRESS minus CONTROL.

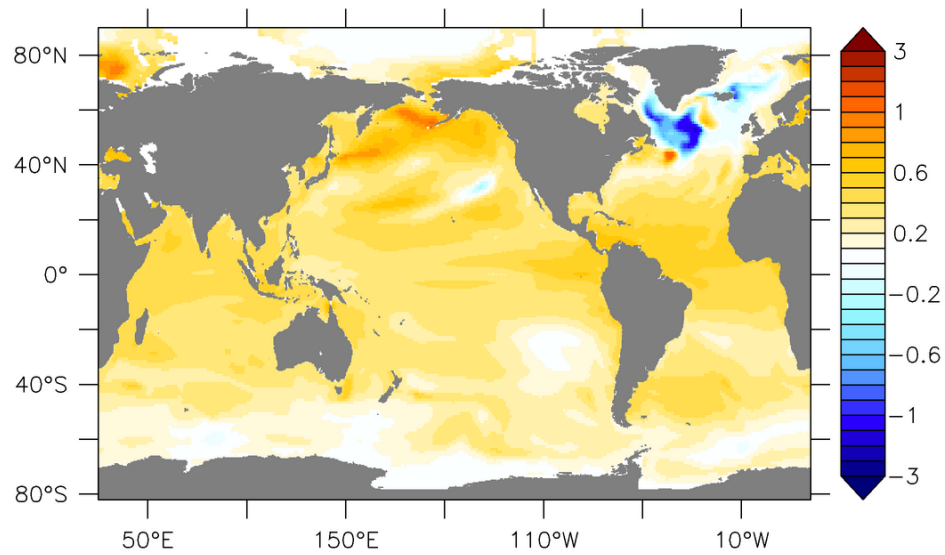


Figure 5 Estimate of SST response(units are K) to radiative forcing change using the ALLFORC experiment with the CM2.1 model. The estimate is calculated as the 10-member ensemble mean SST for the 2002-2012 period minus the 10-member ensemble mean SST for the 1979-2000 period. The negative values in the subpolar North Atlantic are associated with a weakening of the Atlantic Meridional Overturning Circulation.

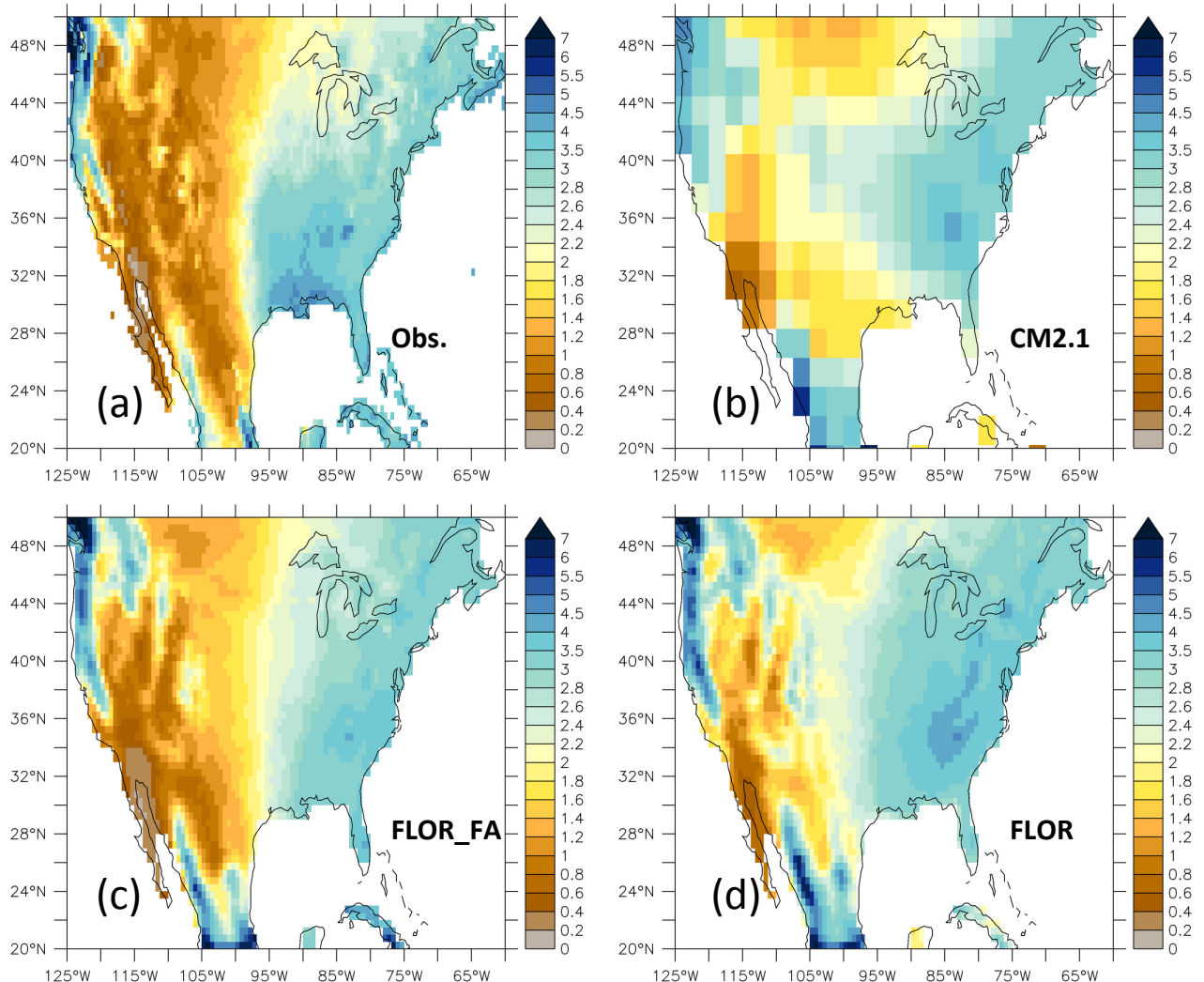


Figure 6 Precipitation climatology from observations and the models. Annual-mean precipitation is shown, units are  $\text{mm day}^{-1}$ . (a) Observations from Climatic Research Unit, University of East Anglia. (b) CM2.1 model. (c) FLOR\_FA model, (d) FLOR model.

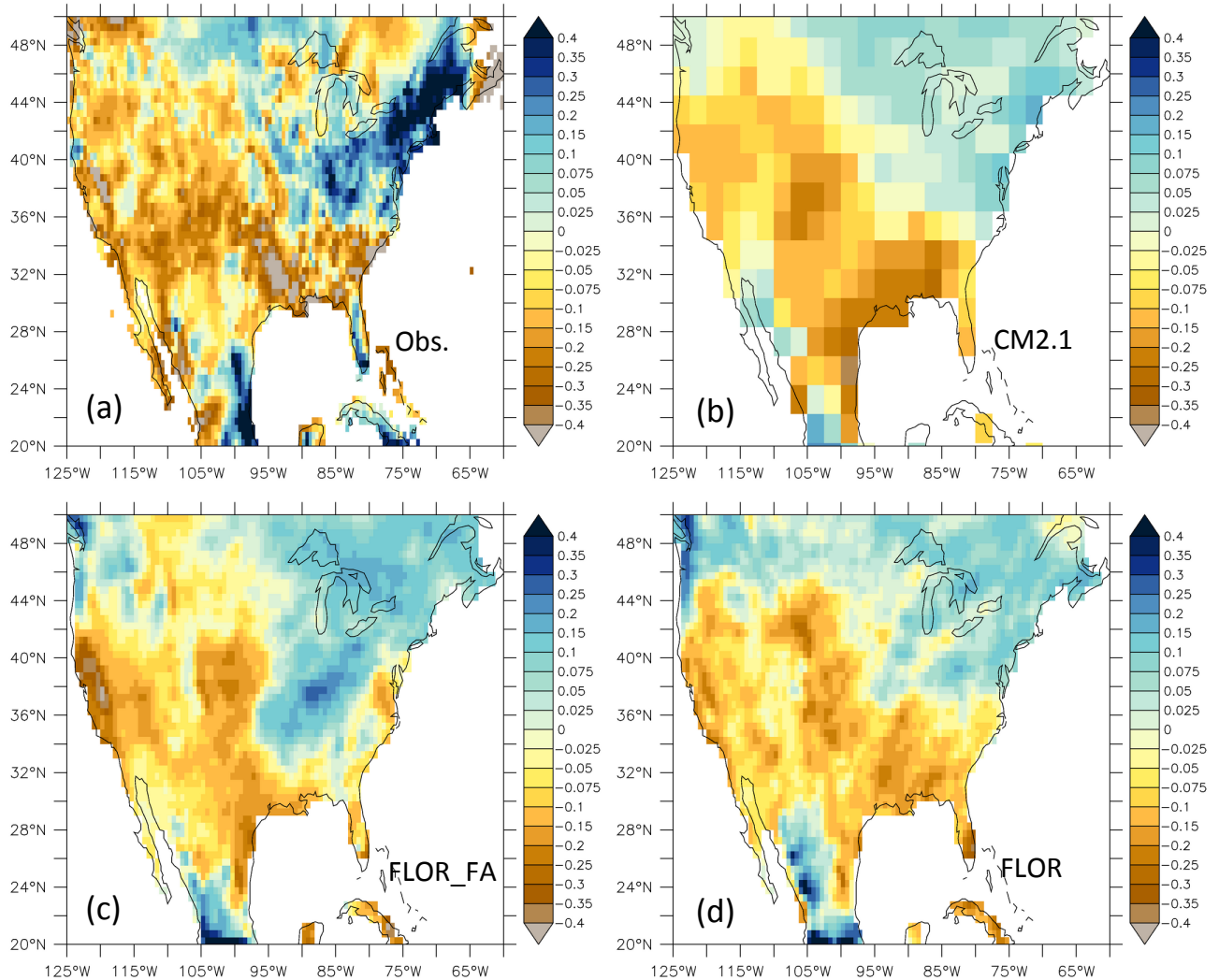


Figure 7 (a) Difference in observed annual mean precipitation for the period 2002-2012 minus 1979-2000. Observations are from the Climatic Research Unit of the University of East Anglia. Units are  $\text{mm day}^{-1}$ . (b) Same as (a) using model results from CM2.1 ALLFORC\_STRESS, showing the combined effects of wind stress and radiative forcing changes. (c) Same as (b) using FLOR\_FA. (d) Same as (b) using FLOR.

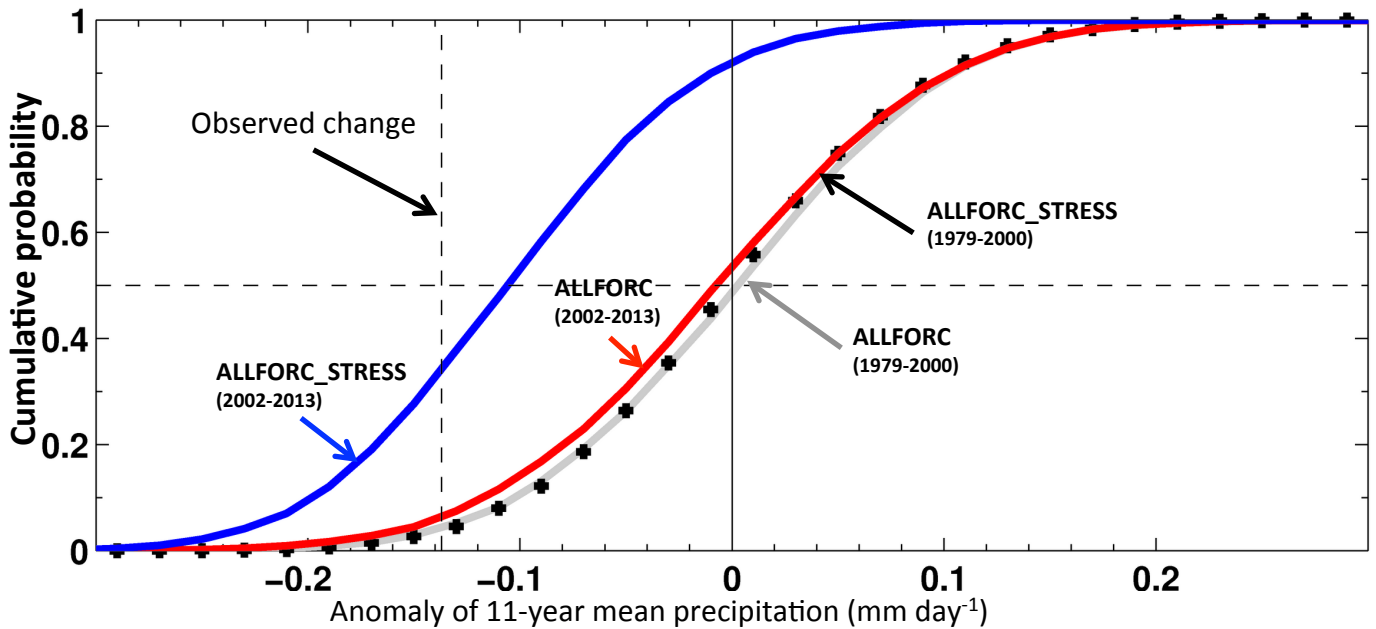


Figure 8 Cumulative probability distribution of 11-year mean precipitation anomalies ( $\text{mm day}^{-1}$ ) averaged over  $130^{\circ}\text{W}-95^{\circ}\text{W}$ ,  $30^{\circ}\text{N}-42^{\circ}\text{N}$ , land only. Grey curve (black crosses) indicates results using model values from the period 1979-2000 from experiment ALLFORC (ALLFORC\_STRESS) using all three models (CM2.1, FLOR, FLOR\_FA). Red (blue) curve denotes values from ALLFORC (ALLFORC\_STRESS) over the period 2002-2012. The distributions are generated by resampling all ensemble members from each model (CM2.1, FLOR, FLOR\_FA) for the experiment and period indicated. For example, for the grey curve we use output from all ten ensemble members of experiment ALLFORC, as well as five ensemble members each from FLOR and FLOR\_FA, over the period 1979-2000 (440 total points, based on 22 years and 10 ensemble members from CM2.1, and 5 ensemble members for 22 years for FLOR and FLOR\_FA respectively). We randomly pick 11 different values from among this pool of 440 values, and then average those to form an 11-year mean, and then subtract from that the ensemble mean value over the period 1979-2000. We repeat this process 10,000 times to form a distribution of 11-year mean anomalies, and plot that as a cumulative probability distribution function. We repeat this process using years 1979-2000 from ALLFORC\_STRESS, years 2002-2012 from ALLFORC, and years 2002-2012 from ALLFORC\_STRESS.

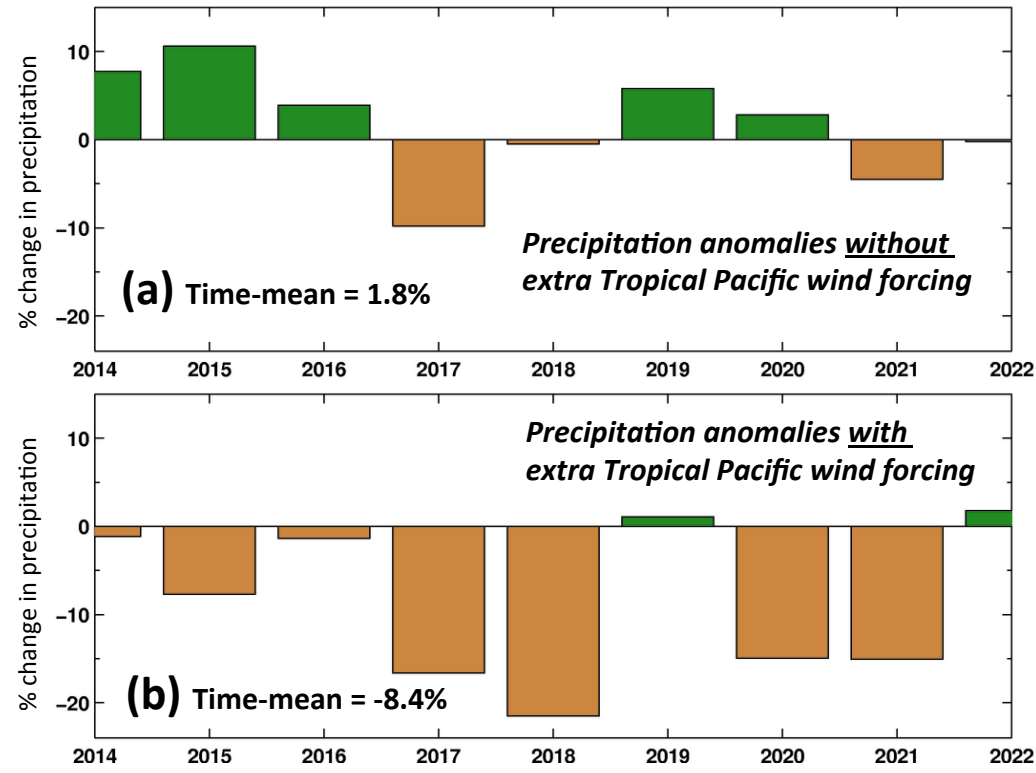


Figure 9 Time series of simulated percentage change in annual mean precipitation relative to the 1979-2000 time-mean, spatially averaged over  $130^{\circ}\text{W}$ - $90^{\circ}\text{W}$ ,  $30^{\circ}\text{N}$ - $42^{\circ}\text{N}$  (land only). The simulations used the CM2.1 model, were 10-member ensembles, and started from identical initial conditions at the end of experiment ALLFORC\_STRESS. (a) Precipitation change with no wind forcing anomaly in tropical Pacific. (b) Precipitation change when observed wind stress anomalies over the period 2005-2013 are applied to the model over the period 2014-2022.

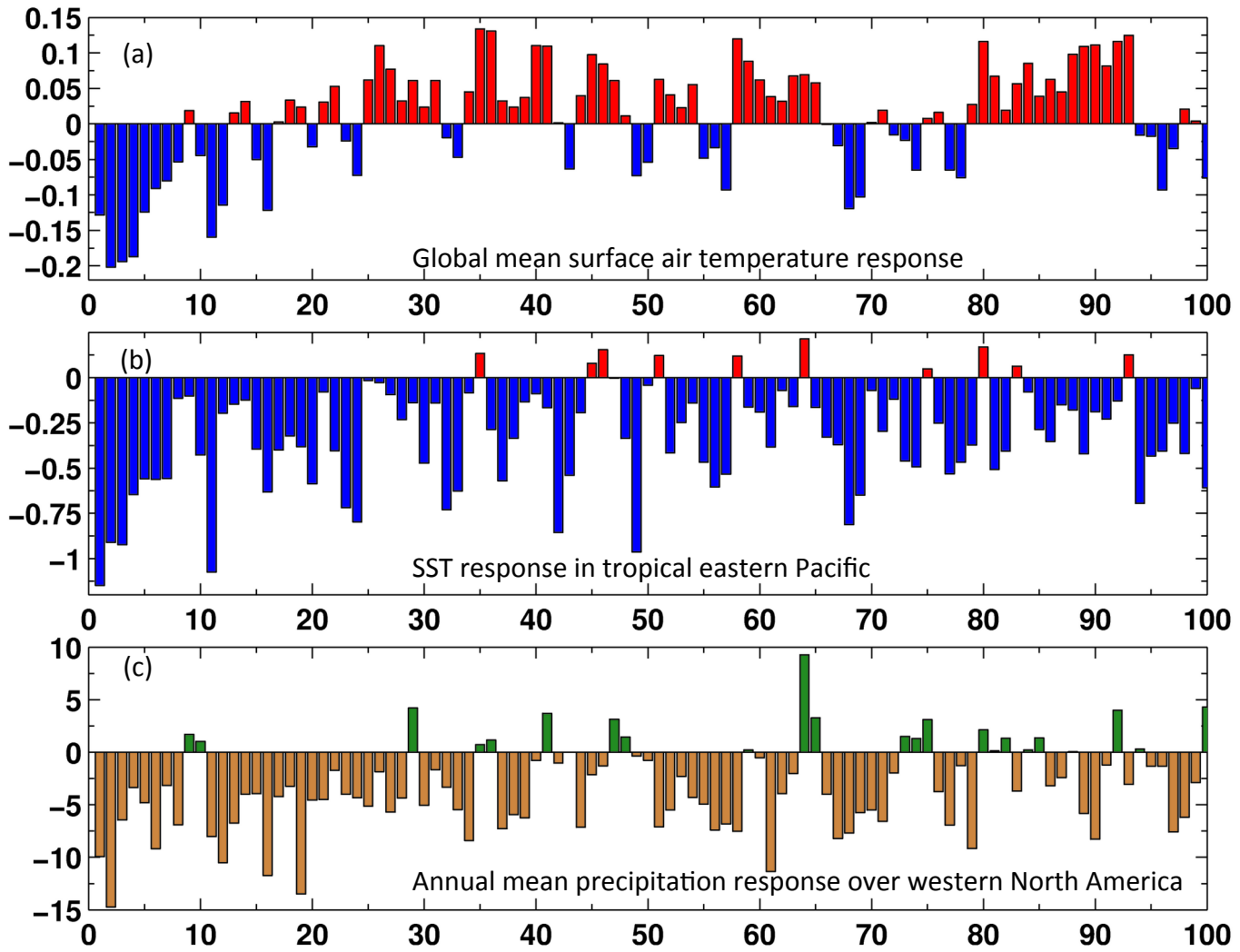


Figure 10 Response of temperature and precipitation to sustained addition of anomalous easterly wind stress in the tropical Pacific. (a) Time series of global mean surface air temperature response, calculated as global mean temperature in CONTROL\_STRESS minus CONTROL. (b) Same as (a), but for SST averaged over a portion of the tropical eastern Pacific ( $170^{\circ}\text{W}$ - $100^{\circ}\text{W}$ ,  $10^{\circ}\text{S}$ - $10^{\circ}\text{N}$ ). (c) Same as (a), but for annual mean rainfall averaged over  $130^{\circ}\text{W}$ - $90^{\circ}\text{W}$ ,  $30^{\circ}\text{N}$ - $42^{\circ}\text{N}$ , land areas only, expressed as percentage change from long-term mean.

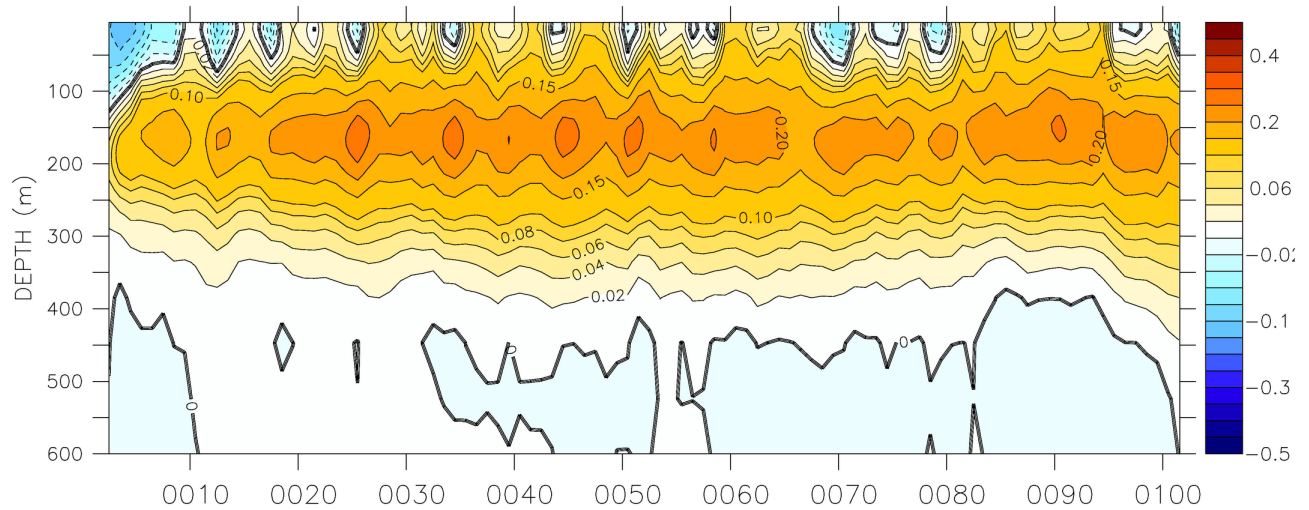


Figure 11 Response of global mean ocean temperature to sustained addition of anomalous easterly wind stress in the tropical Pacific, calculated as experiment CONTROL\_STRESS - CONTROL. Positive values indicate a warming of the ocean in response to the anomalous easterlies.